Submitted to Nuclear Physics A

COULOMB EFFECTS IN RELATIVISTIC NUCLEAR COLLISIONS

M. Gyulassy and S. K. Kauffmann

March 1980

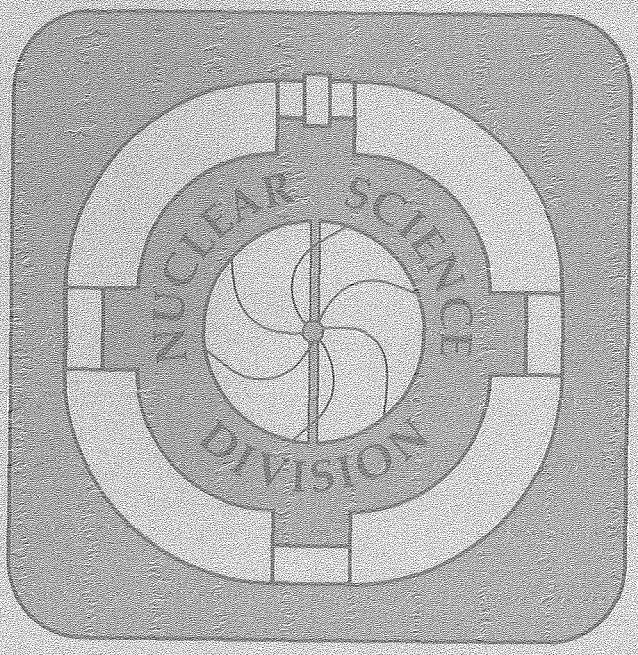

Prepared for the U.S. Department of Energy under Contract W-7405-ENG-48

DISCLAIMER

LBL-10279

COULOMB EFFECTS IN RELATIVISTIC NUCLEAR COLLISIONS

M. Gyulassy and S. K. Kauffmann

Nuclear Science Division
Lawrence Berkeley Laboratory
University of California
Berkeley, CA 94720

Abstract:

We derive simple analytical formulas for Coulomb final state interactions and apply them to the analysis of recent data on nuclear collisions. The π^-/π^+ ratio, the π^+ inclusive cross section, and the n/p ratio are studied. A relativistic field theoretic model is used to derive the formulas to first order in $Z\alpha$. Then based on certain well known non-perturbative results, we recast those formulas in an approximate non-perturbative form to increase their domain of applicability and remove unphysical singularities arising from perturbation theory. The final formulas are covariant and take into account multiple independently moving charged fragments of finite size and finite thermal expansion velocities. Our studies demonstrate analytically the complexity and importance of Coulomb distortions in nuclear collisions.

I. Introduction

Recent data on nuclear collisions in the 1 GeV/nucleon range have revealed unusual angular and momentum magnitude distributions of single particle fragments such as $\pi^{\pm}$, p, n. While it is tempting to attribute those unusual features to nuclear compression effects, it has become increasingly clear that Coulomb final state interactions in nuclear collisions are complex and have to be understood before any conclusions on the role of nuclear compressions can be reached. In this paper we derive simple analytical "pocket" formulas to calculate Coulomb distortions and apply them to the analysis of recent data.

The importance of Coulomb effects was first clearly demonstrated by Benenson et al.[1] in measurements of the π^-/π^+ ratio at $\theta_{lab} = 0$. They found a sharp peak in this ratio for pion velocities close to the velocity of the incident projectile. By comparing the $\pi^{\pm}$ Coulomb wavefunctions in the field generated by the moving projectile fragment, they were able to account qualitatively for that observation. Further evidence for the importance of Coulomb effects was pointed out by Bertsch[2] in explaining the dependence of the π^-/π^+ ratio on the incident bombarding energy.

A third striking effect of Coulomb final state interactions was demonstrated by Libbrecht and Koonin.[3] They showed that in the Coulomb field generated by two relatively moving charged fragments (the projectile and target remnants), a Coulomb focusing effect could arise toward $\theta_{cm} = 90^\circ$ and finite $p_\perp$. With this focusing effect, they were able to account for the broad peak observed in the π^+ spectra near $\theta_{cm} = 90^\circ$ and $p_\perp \approx m_\pi/2$. The method used for that analysis was

the numerical solution of classical equations of motion in the time dependent field of the moving fragments.

This paper aims at supplementing and extending these previous works by deriving analytical formulas that clearly reveal the structure and form of Coulomb distortions in nuclear collisions. Our basic approach is to use first order relativistic perturbation theory. With this approach we readily obtain an expression for Coulomb distortions for an arbitrary space-time dependent charge current. In particular, effects due to finite nuclear sizes and expanding (time dependent) fireballs are easily calculated. The formula naturally incorporates multiple, independently moving charged fragments as well. Therefore, the Coulomb effects from the combined fields of the projectile and target remnants as well as the expanding fireball are taken into account. To overcome some of the limitations of perturbation theory, we proceed to recast our results in a non-perturbative (Gamow factor[6]) form that becomes exact for a single static point charge. In this way, quantum effects, that are in fact important only when finite size effects become negligible, are well approximated in a non-perturbative way. Also, the unphysical singularities of the perturbative results are eliminated by this non-perturbative extension.

The subsequent sections are organized as follows: In Section II, simple classical arguments are presented that reveal the qualitative effect of Coulomb final state interactions. A dual aspect of the

Coulomb distortion is emphasized. First, there is a Coulomb impulse, $\delta\underset{\sim}{p}$, which tends to enhance the positively charged fragments relative to the neutrals. Second, there is a Coulomb phase space distortion, $D(\underset{\sim}{k})$, which tends to suppress the positively charged fragments relative to the neutrals. The competing roles of these two effects is a recurring theme throughout this paper. In Section III, we use the results of an exactly soluble field theoretic model[7] to calculate relativistic and quantum effects to first order in $Z\alpha$. The non-perturbative extension of those formulas is then motivated and carried out. In Section IV, we apply our formulas to the analysis of the π^-/π^+ ratio[1], the π^+ spectra[4,5], and the n/p ratio[8] in nuclear collisions. Finally, concluding remarks are presented in Section V.

(Note that we use $\hbar = c = 1$ units and the $(ab) = a_\mu b^\mu = a_o b_o - \underset{\sim}{a}\cdot\underset{\sim}{b}$ convention.)

II. Classical Considerations

Classically, final state interactions lead simply to a change of variables, $\underset{\sim}{k}_0(\underset{\sim}{k})$, from an initial momentum $\underset{\sim}{k}_0$ to a final momentum k. The form of $\underset{\sim}{k}_0(\underset{\sim}{k})$ is obtained by integrating Newton's equations as in Ref. (3). Once $\underset{\sim}{k}_0(\underset{\sim}{k})$ is known, then the single particle inclusive cross sections, $\sigma(\underset{\sim}{k}) = d^3\sigma/dk^3$, for charged particles can be related to the inclusive cross section, $\sigma_0(\underset{\sim}{k}) = d^3\sigma_0/dk^3$, for neutral particles via this change of variables as

$$\sigma(\underset{\sim}{k}) = \sigma_0(\underset{\sim}{k}_0(\underset{\sim}{k}))\left|\frac{\partial^3 k_0}{\partial^3 k}\right| \quad . \tag{2.1}$$

There are clearly two distinct effects arising from final state interactions in Eq. (2.1). First, there is a momentum shift of the argument of σ_0 given by

$$\pm\delta\underset{\sim}{p}(\underset{\sim}{k}) = \underset{\sim}{k} - \underset{\sim}{k}_0(\underset{\sim}{k}) \tag{2.2}$$

for $\pm$ charged particles due to accelerations or decelerations in the external Coulomb fields. Second, there is a change in the density of states in momentum space expressed via the Jacobian, $\left|\partial^3 k_0/\partial^3 k\right|$. This Jacobian will be referred to as the Coulomb phase space factor.

As an instructive example of Eq. (2.1), consider the Coulomb distortion due to a positive static, spherically symmetric charge distribution whose total charge is $Z|e|$ and whose mean inverse radius,

$\langle r^{-1} \rangle^{-1}$, is R. The resulting Coulomb potential at the origin has the value $|e|V(0) = Z\alpha/R$. For $\pm|e|$ charged particles of mass m emitted from the origin, energy conservation leads to

$$\underset{\sim}{k}_0(\underset{\sim}{k}) = \underset{\sim}{k}\left(1 \mp k_c^2/k^2\right)^{1/2} ,$$

$$\left|\frac{\partial^3 k_0}{\partial^3 k}\right| = \frac{k_0(k)}{k} = \left(1 \mp k_c^2/k^2\right)^{1/2} , \qquad (2.3)$$

where $k_c = (2mZ\alpha/R)^{1/2}$ is the Coulomb barrier impulse. Below k_c there are no classically allowed states for + charged particles. For a Coulomb free thermal distribution, $\sigma_0(k) \propto \exp(-k^2/2mT)$, as in the fireball model,[9] and the Coulomb distorted cross sections for $\pm$ charged particles are therefore

$$\sigma_\pm(\underset{\sim}{k}) = \sigma_0(\underset{\sim}{k})\, e^{\pm Z\alpha/RT} \left(1 \mp k_c^2/k^2\right)^{1/2}$$

$$\approx \sigma_0(\underset{\sim}{k})\left\{1 \pm \left(\frac{Z\alpha}{RT} - \frac{mZ\alpha}{k^2 R}\right)\right\} , \qquad (2.4)$$

where we expanded $\sigma_\pm(\underset{\sim}{k})$ in the last line to first order in $Z\alpha$. Equation (2.4) illustrates the competing roles of the momentum shift, $\underset{\sim}{\delta p}$, which <u>increases</u> the cross section of protons relative to neutrons, and the Coulomb phase space factor, $\left|\partial^3 k_0/\partial^3 k\right|$, which <u>reduces</u> the proton yield. For low momenta, $k < \sqrt{mT}$, in the fireball frame, the Coulomb phase space distortion dominates, and the neutron to proton, n/p, ratio

and the π^-/π^+ ratio are greater than unity. On the other hand, for $k > \sqrt{mT}$, the Coulomb impulse dominates, and $n/p < 1$ and $\pi^-/\pi^+ < 1$.

This competing effect of the Coulomb impulse and Coulomb phase space is a basic and general feature that we also find in the relativistic quantum treatment of Section III.

If the charge density producing the Coulomb field is set in uniform motion with velocity $\underset{\sim}{v}_1$ relative to the fireball source, then a simple Galilean transformation of Eq. (2.3) gives for $\pm$ charged particles

$$\underset{\sim}{k}_o(\underset{\sim}{k}) = \underset{\sim}{k} \mp \delta\underset{\sim}{p}(\underset{\sim}{k} - \underset{\sim}{k}_1) = (\underset{\sim}{k} - \underset{\sim}{k}_1) \left\{1 \mp \frac{k_c^2}{|\underset{\sim}{k} - \underset{\sim}{k}_1|^2}\right\}^{1/2} + \underset{\sim}{k}_1 \quad , \quad (2.5)$$

where $\underset{\sim}{k}_1 = m\underset{\sim}{v}_1$ and to lowest order in $Z\alpha$, the momentum shift is given by

$$\delta\underset{\sim}{p}(\underset{\sim}{k} - \underset{\sim}{k}_1) = (\underset{\sim}{k} - \underset{\sim}{k}_1) \frac{Z\alpha m}{|\underset{\sim}{k} - \underset{\sim}{k}_1|^2 R} \quad . \quad (2.6)$$

Furthermore, the Coulomb phase space distortion factor is then given by

$$\left|\frac{\partial k_o^3}{\partial k^3}\right| = 1 \mp \delta D(k - k_1)$$

$$= \left\{1 \mp \frac{k_c^2}{|\underset{\sim}{k} - \underset{\sim}{k}_1|^2}\right\}^{1/2} \quad , \quad (2.7)$$

where to lowest order, the distortion factor is

$$\delta D(\underset{\sim}{k} - \underset{\sim}{k}_1) = \frac{Z\alpha m}{|\underset{\sim}{k} - \underset{\sim}{k}_1|^2 R} = \underset{\sim}{\nabla} \cdot \delta \underset{\sim}{p}(\underset{\sim}{k}) \Big]_{\underset{\sim}{k}-\underset{\sim}{k}_1} \quad . \tag{2.8}$$

Evaluating the charged particle cross sections via Eq. (2.1), the π^-/π^+ ratio for a given $\underset{\sim}{k}$ in the fireball frame is then given to first order in $Z\alpha$ by

$$\frac{\pi^-(\underset{\sim}{k})}{\pi^+(\underset{\sim}{k})} = 1 - 2\left[\frac{\underset{\sim}{k} \cdot \delta \underset{\sim}{p}(\underset{\sim}{k} - \underset{\sim}{k}_1)}{mT} - \delta D(\underset{\sim}{k} - \underset{\sim}{k}_1)\right]$$

$$= 1 - \frac{2Z\alpha}{R}\left[\frac{\underset{\sim}{k} \cdot (\underset{\sim}{k} - \underset{\sim}{k}_1)}{T|\underset{\sim}{k} - \underset{\sim}{k}_1|^2} - \frac{m}{|\underset{\sim}{k} - \underset{\sim}{k}_1|^2}\right] \quad . \tag{2.9}$$

The n/p ratio is given by a similar expression. If the charge density were at rest relative to the fireball, then $\underset{\sim}{k}_1 = 0$, and Eq. (2.9) is equivalent to Eq. (2.4). However, if $\underset{\sim}{k}_1 \neq 0$ then the π^-/π^+ ratio peaks for pion momentum, $\underset{\sim}{k} = \underset{\sim}{k}_1$, which corresponds to zero relative velocity in the charge density frame. This feature is clearly seen in the Benenson et al. data.[1] On the other hand, for $k >> k_1$, $\delta D \to 0$, and the impulse term, $\underset{\sim}{k} \cdot \delta \underset{\sim}{p}(\underset{\sim}{k})$, dominates. In that case, $\pi^-/\pi^+ \to 1 - 2Z\alpha/RT$, as derived in another way by Bertsch.[2] While Eq. (2.9) exhibits the main qualitative features of the π^-/π^+ data, important quantum corrections arise for $|\underset{\sim}{k} - \underset{\sim}{k}_1| < 1/R$. These corrections are calculated in Section III.

There is another basic effect which may be derived from simple classical considerations. Consider a charge density that arises from a freely expanding thermal source:

$$\rho(\underset{\sim}{x},t) = \int d^3x_o d^3v_o \rho_f(\underset{\sim}{x}_o)\ f(\underset{\sim}{v}_o)\ \delta^3(\underset{\sim}{x} - \underset{\sim}{x}_o - \underset{\sim}{v}_o t)$$

$$= \int d^3\underset{\sim}{v}_o\ f(\underset{\sim}{v}_o)\ \rho_f(\underset{\sim}{x} - \underset{\sim}{v}_o t) \quad . \tag{2.10}$$

Equation (2.10) describes a freely expanding gas of protons that at $t = 0$ were distributed in space according to a freezout density,[9] $\rho(\underset{\sim}{x},t=0) = \rho_f(\underset{\sim}{x})$, and a velocity distribution $f(\underset{\sim}{v}_o)$ independent of position. The remarkable feature seen in the second line of Eq. (2.10) is that this expanding charge density is equivalent to an ensemble of uniformly translating freezout densities! This simple property allows us to calculate immediately the Coulomb impulse and distortion to first order from Eqs. (2.6) and (2.8) as

$$\delta\underset{\sim}{p}_f(\underset{\sim}{k}) = \int d^3v_o f(\underset{\sim}{v}_o)\ \delta\underset{\sim}{p}(\underset{\sim}{k} - m\underset{\sim}{v}_o) \approx \underset{\sim}{k}\ \frac{Z\alpha m}{(k^2 + k_T^2)\ R} \quad , \tag{2.11}$$

and

$$\delta D_f(\underset{\sim}{k}) = \int d^3v_o f(\underset{\sim}{v}_o)\ \delta D(\underset{\sim}{k} - m\underset{\sim}{v}_o) \approx \frac{Z\alpha m}{(k^2 + k_T^2)R} \quad , \tag{2.12}$$

For simplicity, we have assumed $f(\underset{\sim}{v}_o) = f(|\underset{\sim}{v}_o|)$, as for thermal protons, and approximated the integrations by replacing $|\underset{\sim}{k} - m\underset{\sim}{v}_o|^2$ in the denominators by $\langle|\underset{\sim}{k} - m\underset{\sim}{v}_o|^2\rangle = k^2 + k_T^2$. The thermal average momentum is

$k_T^2 = \int f(v_o)(mv_o)^2 = 3mT(m/m_p)$, where m is the mass of the detected particle, T is the temperature of the proton gas, and m_p is the proton mass.

It is clear from Eqs. (2.11)and (2.12) that a finite expansion rate reduces both the Coulomb impulse and distortion factor. Physically, this follows from the fact that the time averaged electric fields are smaller for an expanding charge source than a static one.

For a uniformly translating fireball, Eqs. (2.11) and (2.12) must be evaluated with the Galilean transformed $\underset{\sim}{k} \to \underset{\sim}{k} - \underset{\sim}{k}_f$, where $\underset{\sim}{k}_f/m$ is the cm velocity of the fireball.

Finally, for several independent fireball charge distributions specified by charges Z_i, cm velocities $\underset{\sim}{k}_i/m$, thermal expansion velocities k_{T_i}/m, and freezout radii R_i, the charged particle cross sections are given to first order by

$$\sigma_{\pm}(\underset{\sim}{k}) = \sigma_o(\underset{\sim}{k})\{1 \mp \delta D(\underset{\sim}{k})\} \mp \delta\underset{\sim}{p}(\underset{\sim}{k})\cdot\underset{\sim}{\nabla}\sigma_o(\underset{\sim}{k})$$

$$\approx \sigma_o(\underset{\sim}{k} \mp \delta\underset{\sim}{p}(\underset{\sim}{k}))\ D(\underset{\sim}{k}) \quad , \tag{2.13}$$

where we rewrote the first order result in the canonical form, Eq. (2.1). For this multiple fireball case, the Coulomb impulse is given by

$$\delta\underset{\sim}{p}(\underset{\sim}{k}) = \sum_i \frac{(\underset{\sim}{k} - \underset{\sim}{k}_i)}{(\underset{\sim}{k} - \underset{\sim}{k}_i)^2 + k_{T_i}^2} \frac{Z_i \alpha m}{R_i} \quad , \tag{2.14}$$

and the Coulomb phase space distortion factor is given by

$$D(\underset{\sim}{k}) = \left\{1 \mp 2\sum_i \frac{Z_i \alpha m}{R_i} \frac{1}{(\underset{\sim}{k} - \underset{\sim}{k}_i)^2 + k_{T_i}^2}\right\}^{1/2} . \qquad (2.15)$$

It is important to note that Eqs. (2.13)-(2.15) are strictly valid only to lowest order in $Z\alpha$ in the classical, non-relativistic limit. However, by rewriting them in the canonical form we gain an extrapolation formula incorporating some higher order effects. In practice, comparison of the results from the first and second line in Eq. (2.13) provides a useful estimate of the magnitude of higher order corrections $O((Z\alpha)^2)$ to the first order results. As we show in Section III, quantum corrections to Eqs. (2.14) and (2.15) arise when $|\underset{\sim}{k} - \underset{\sim}{k}_i| < 1/R_i$ for some source i, and relativistic corrections enter for large relative momenta $|\underset{\sim}{k} - \underset{\sim}{k}_i| \gtrsim m$. Nevertheless, Eqs. (2.13)-(2.15) reveal already the most important qualitative features of Coulomb distortions in nuclear collisions.

III. Relativistic Quantum Analysis

A. The Single $\pi^{\pm}$ Inclusive

We calculate now Coulomb distortions within the following exactly solvable field theoretic model of multi-pion production:

$$\mathcal{L}(x) = |(i\partial_\mu - eA_\mu(x))\,\phi(x)|^2 - m_\pi^2\phi^+(x)\phi(x) + J(x)\,\phi^+(x) + J^*(x)\phi(x) \qquad (3.1)$$

In Eq. (3.1), $\phi(x)$ is the π^- field operator. The (c-number) source current $J(x)$ of the pions is taken as a given function of x_μ related to the expectation value of the nuclear pseudoscalar current, $\langle\bar{\psi}(x)\,\gamma_5\tau_-\,\psi(x)\rangle$.

In addition, the (c-number) electromagnetic field $A_\mu(x)$ is generated by a given nuclear charge current, $Z|e|j_\mu(x)$, via Maxwell's equations:

$$|e|A_\mu(q) = -\frac{4\pi Z\alpha}{q^2 + i\epsilon}\,j_\mu(q) \qquad . \qquad (3.2)$$

Of course, the current also satisfies the continuity equation, $q^\mu\,j_\mu(q) = 0$.

This model, Eq. (3.1), was motivated and studied in detail in Ref. (7) in connection with multipion inclusive cross sections for nuclear collisions. For our purposes, we only quote the results for the invariant single π^- inclusive cross section

$$\sigma(\underset{\sim}{k}) = \omega_k\,\frac{d^3\sigma}{dk^3} = |J_A(k)|^2\,\sigma_\pi \quad , \qquad (3.3)$$

with $\omega_k = (k^2 + m_\pi^2)^{1/2}$, σ_π is the total negative π production cross section, and the production amplitude is

$$J_A(\underset{\sim}{k}) = \int d^4x \; J(x) \, \psi^*_{\underset{\sim}{k}}(x) \quad . \tag{3.4}$$

The incoming pion wavefunction in Eq. (3.4) satisfies

$$((i\partial_\mu - eA_\mu)^2 - m_\pi^2) \, \psi_{\underset{\sim}{k}}(x) = 0 \quad , \tag{3.5}$$

together with the boundary condition

$$\lim_{x_0 \to +\infty} \psi_{\underset{\sim}{k}}(\underset{\sim}{x}, x_0) = f_{\underset{\sim}{k}}(x) = \frac{e^{-ikx}}{\sqrt{2(2\pi)^3}} \quad . \tag{3.6}$$

In the absence of final state interactions, $A_\mu = 0$, $\psi_{\underset{\sim}{k}}(x) = f_k(x)$ for all times, and $J_A(\underset{\sim}{k})$ is proportional to the Fourier transform, $J(\underset{\sim}{k}, \omega_k)$, of $J(\underset{\sim}{x}, x_0)$. In this case, the invariant π^- cross section simply measures the modulus square of $J(\underset{\sim}{k}, \omega_k)$ as

$$\sigma_0(\underset{\sim}{k}) = \frac{|J(\underset{\sim}{k}, \omega_k)|^2}{2(2\pi)^3} \, \sigma_\pi \quad . \tag{3.7}$$

The π^+ cross section is obtained via crossing ($k_\mu \to -k_\mu$). (For N = Z systems $J(k) = J(-k)$, and the $\pi^\pm$ cross sections are the same in the absence of Coulomb effects.)

Equation (3.4) has the simple physical interpretation that the amplitude, $J_A(\underset{\sim}{k})$, to observe a pion with momentum $\underset{\sim}{k}$ at infinity in the presence of a field $A_\mu(x)$ is equal to amplitude $J(x)$ to create

the pion at position x_μ times the amplitude $\psi^*_{\underset{\sim}{k}}(x)$ for that pion to be found with momentum $\underset{\sim}{k}$ at time $+\infty$.

Equations (3.3)-(3.6) formally solve the problem of Coulomb distortions. However, in practical cases, where $A_\mu(x)$ describes the field due to many independently moving source,[3] Eq. (3.5) can only be solved numerically. Since our aim here is to gain analytical insight into the complex nature of Coulomb distortions, we turn to perturbation theory.

Converting Eqs. (3.5) and (3.6) into an integral equation, $\psi^*_{\underset{\sim}{k}}$ is given to first order in $Z\alpha$ by

$$\psi^*_{\underset{\sim}{k}}(x) \approx f^*_{\underset{\sim}{k}}(x) + \delta\psi^*_{\underset{\sim}{k}}(x)/\sqrt{2(2\pi)^3} \quad , \tag{3.8}$$

where

$$\begin{aligned}\delta\psi^*_{\underset{\sim}{k}}(x) &= 2e \int d^4y\, e^{iky}\, k_\mu A^\mu(y)\, \Delta_\pi(y - x) \\ &= \int \frac{d^4q}{(2\pi)^4}\, e^{i(q+k)x}\, \Delta_\pi(q + k)\, 2ek_\mu A^\mu(-q) \quad ,\end{aligned} \tag{3.9}$$

with $\Delta_\pi^{-1}(q) = (q^2 - m_\pi^2 + i\epsilon)$.

To first order in $Z\alpha$, Eq. (3.4) becomes

$$J_A(\underset{\sim}{k}) = (J(\underset{\sim}{k},\omega_k) + \delta J(\underset{\sim}{k},\omega_k))/\sqrt{2(2\pi)^3} \quad , \tag{3.10}$$

with the change in the production amplitude given by

$$\delta J(k) = \int \frac{d^4q}{(2\pi)^4} J(q + k)\, \Delta_\pi(q + k)\, 2ek_\mu A^\mu(-q) \quad . \tag{3.11}$$

We now simplify Eq. (3.11) by noting that $A^\mu(q)$ in Eq. (3.2) is a sharply peaked function of q_μ centered at $q_\mu = 0$. For a static charge density, with a radius R, the current, $j_\mu(q) = \delta_{\mu o}\, 2\pi\, \delta(q_o)\, \rho(\underset{\sim}{q})$, restricts the domain of integration to momenta $|\underset{\sim}{q}| \lesssim 1/R$. On the other hand, J(q) is a slowly varying function on a larger momentum scale, $\sim m_\pi$, for nuclear collisions.

So long as $1/R \ll m_\pi$, it will be useful to expand J(q + k) in Eq. (3.11) in a Taylor series about q = 0. Expanding to first order in the gradient of J(k), we have then

$$\delta J(k) \approx \int \frac{d^4q}{(2\pi)^4} \left(J(k) + q_\nu \partial^\nu J(k)\right) \Delta_\pi(q + k)\, 2ek_\mu A^\mu(-q)$$

$$= \left\{ J(k) + \frac{\partial}{\partial k_\nu} J(k) \left(-i \frac{\partial}{\partial x^\nu} - k_\nu \right) \right\} \delta\psi^*_{\underset{\sim}{k}}(x = 0) \quad , \tag{3.12}$$

where $\delta\psi^*$ is given by Eq. (3.9). The first term incorporates the change in the probability amplitude to find the pion at the creation point $x_\mu = 0$. The second term incorporates the change in the momentum density at $x_\mu = 0$ due to the Coulomb forces. This term allows some of the off shell pions ($k^o \neq \omega_k$) produced by the source $J(\underset{\sim}{k}, k^o)$ to materialize after absorbing the necessary four momentum from the Coulomb field. In addition, it allows the pion at the creation point $x_\mu = 0$ to have some initial three momentum $\underset{\sim}{k}_o$ that

is different from the finally observed one, $\underset{\sim}{k}$, in accord with our classical intuition.

Inserting Eq. (3.12) into Eq. (3.10), we obtain from Eq. (3.3) the charged pion inclusive cross section to first order in $Z\alpha$ and to first order in the gradient of J(k) as

$$\begin{aligned}\sigma_{\pm}(k) &\approx \frac{\sigma_{\pi}}{2(2\pi)^3}\left\{|J(k)|^2 + 2\mathrm{Re}J^{*}(k)\delta J(k)\right\} \\ &\approx \sigma_0(k)\left\{1 \mp \delta D(k)\right\} \mp \delta p_{\nu}(k)\frac{\partial}{\partial k_{\nu}}\sigma_0(k) \\ &\approx \sigma_0(k \mp \delta p(k))\left\{1 \mp \delta D(k)\right\} \quad , \end{aligned} \tag{3.13}$$

where $\sigma_0(\underset{\sim}{k},k^0) = \sigma_{\pi}|J(\underset{\sim}{k},k^0)|^2/(2(2\pi)^3)$. For $k^0 = \omega_k = (k^2 + m^2)^{1/2}$, $\sigma_0(\underset{\sim}{k},\omega_k)$ is identical to the neutral particle cross section in Eq. (3.7). In the last line of Eq. (3.13) we have expressed $\sigma_{\pm}(k)$ in the canonical form of Eq. (2.13) so as to make the physical interpretation of δp and δD immediately clear.

From Eqs. (3.12) and (3.13), the distortion factor is given by

$$\begin{aligned}\delta D(k) &= 2\ \mathrm{Re}\ \delta\psi^{*}_{\underset{\sim}{k}}(x = 0) \\ &= 16\pi\ Z\alpha\ \mathrm{Re}\int\frac{d^4q}{(2\pi)^4}\,\Delta_{\pi}(k + q)\,\frac{k^{\mu}j_{\mu}(-q)}{q^2 + i\epsilon} \quad , \end{aligned} \tag{3.14}$$

and the four momentum impulse is given by

$$\delta p_\nu(k) = 8\pi Z\alpha \, \mathrm{Re} \int \frac{d^4q}{(2\pi)^4} \, q_\nu \Delta_\pi(k+q) \, \frac{k^\mu j_\mu(-q)}{q^2 + i\epsilon} \quad . \tag{3.15}$$

These are the relativistic quantum expressions to first order in $Z\alpha$, which replace Eqs. (2.6) and (2.8) of the Section II. We turn next to a detailed study of Eqs. (3.14) and (3.15).

B. Static Finite Size Effects

Consider a static charge density,

$$j_\mu(\underset{\sim}{x},t) = \delta_{\mu 0}\rho(\underset{\sim}{x}) \quad , \tag{3.16}$$

Non-static effects are considered in Section III-C. The distortion factor, Eq. (3.14), can then be written as

$$\delta D(k) = \pi \frac{Z\alpha}{\beta_k} \mathcal{F}(\underset{\sim}{k}) \quad , \tag{3.17}$$

where $\beta_k = k/\omega_k$ is the speed of the particle, and the Coulomb form factor is defined as

$$\begin{aligned} \mathcal{F}(\underset{\sim}{k}) &= \frac{\mathrm{Re}}{\pi^3} \int d^3q \, \frac{2|\underset{\sim}{k}|}{2\underset{\sim}{k}\cdot\underset{\sim}{q} + q^2 - i\epsilon} \, \frac{\rho(-\underset{\sim}{q})}{q^2 - i\epsilon} \\ &= \frac{\mathrm{Re}}{\pi^3} \int d^3p \, \frac{2}{2\hat{\underset{\sim}{k}}\cdot\underset{\sim}{p} + p^2 - i\epsilon} \, \frac{\rho(-|\underset{\sim}{k}|\underset{\sim}{p})}{p^2 - i\epsilon} \end{aligned} \tag{3.18}$$

with $\hat{k} = \underset{\sim}{k}/|\underset{\sim}{k}|$ and $\rho(\underset{\sim}{q}) = \int d^3x \, \exp(-i\underset{\sim}{q}\cdot\underset{\sim}{x})\rho(\underset{\sim}{x})$. In the second line, the change of variables $\underset{\sim}{p} = \underset{\sim}{q}/|\underset{\sim}{k}|$ is performed so that the $\underset{\sim}{k} \to \underset{\sim}{0}$ limit is easily evaluated. Noting that $\rho(\underset{\sim}{q} = \underset{\sim}{0}) = 1$ by normalization, we find

$$\mathcal{F}(\underset{\sim}{k}) \longrightarrow 1 \quad , \tag{3.19}$$
$$\underset{\sim}{k}\to\underset{\sim}{0}$$

as verified by direct integration in spherical coordinates.

Comparing to the familiar Gamow factor[6]

$$G(\eta) = |\psi_{\underset{\sim}{k}}(x = 0)|^2 = \frac{2\pi\eta}{e^{2\pi\eta} - 1} \quad , \tag{3.20}$$

where $\eta = \pm Z\alpha/\beta_k$, we see that in the limit $\underset{\sim}{k} \to \underset{\sim}{0}$ the Coulomb phase space factor, $1 \mp \delta D(k)$, becomes identical to $G(\eta)$ to first order in $Z\alpha$ <u>independent</u> of the form of $\rho(\underset{\sim}{x})$. Equation (3.20) is the penetration factor for a static point charge density. That the Coulomb distortion factor for a finite size density reduces to the point charge expression follows, of course, from the quantum property that a particle with momentum $k < 1/R$ cannot resolve the finite size, R, of a system.

On the other hand, for $k > 1/R$, finite size effects do become important, and $\mathcal{F} \neq 1$. The asymptotic, $k \gg 1/R$, form of $\mathcal{F}$ can be derived from Eq. (3.18) via the following expansion of the pion propagator:

$$[2\underset{\sim}{k}\cdot\underset{\sim}{q} + q^2 - i\varepsilon]^{-1} = i\int_0^\infty d\tau\, e^{-i(2\underset{\sim}{k}\cdot\underset{\sim}{q} + q^2)\tau}\, e^{-\varepsilon\tau}$$

$$\approx i\int_0^\infty d\tau\, e^{-\varepsilon\tau}\, e^{-i2\underset{\sim}{k}\cdot\underset{\sim}{q}\tau}\left\{1 - iq^2\tau + O(\tau^2)\right\} \quad . \tag{3.21}$$

With Eq. (3.21), we evaluate Eq. (3.18) in the $k \to \infty$ limit as

$$\mathfrak{F}(\underset{\sim}{k}) \underset{k\to\infty}{\longrightarrow} \mathrm{Re}\,\frac{2ik}{\pi^3}\int_0^\infty d\tau\, e^{-\varepsilon\tau}\int d^3q\, e^{-i2\underset{\sim}{k}\cdot\underset{\sim}{q}\tau}\left\{1 - iq^2\tau\right\} A_0'(-\underset{\sim}{q})$$

$$= 8k\ \mathrm{Im}\int_0^\infty d\tau\left\{-A_0'(\underset{\sim}{x} = \underset{\sim}{k}\tau) + i\,\frac{\tau}{2}\,\rho(\underset{\sim}{x} = \underset{\sim}{k}\tau)\right\}$$

$$= \frac{4}{k}\int_0^\infty d\tau\ \ \tau\rho(\underset{\sim}{x} = \hat{\underset{\sim}{k}}\tau) \qquad . \tag{3.22}$$

where we changed variables $\tau \leftarrow 2\tau$ in the second line and $\tau \leftarrow |\underset{\sim}{k}|\tau$ in the last line. Note that the $iA_0'(k\tau) \equiv iA_0(\underset{\sim}{k}\tau)|e|/4\pi Z\alpha$ term does not contribute to the real part required in Eq. (3.18). Corrections to Eq. (3.22) appear to order $(kR)^{-3}$.

For large k, $\mathfrak{F}$ thus measures the line integral of $\rho(\underset{\sim}{x})$ along a straight line trajectory from $\underset{\sim}{x} = \underset{\sim}{0}$ in the direction $\hat{\underset{\sim}{k}}$. For a spherically symmetric $\rho(\underset{\sim}{x})$, this line integral is, in fact, proportional to the mean inverse radius, $\langle r^{-1}\rangle$, of the charge density. Thus, for a spherically symmetric $\rho(\underset{\sim}{x}) = \rho(|\underset{\sim}{x}|)$,

$$\mathfrak{F}(\underset{\sim}{k}) \underset{\underset{\sim}{k}\to\infty}{\longrightarrow} \frac{1}{\pi kR} \qquad , \tag{3.23}$$

where $R = \langle 1/|\underset{\sim}{x}|\rangle^{-1}$. Thus $\delta D \to Z\alpha/(\beta_k kR)$, which is precisely the classical form, Eq. (2.8), with k/m replaced by the relativistic velocity, k/ω_k.

As an example of the full form of $\mathfrak{F}(\underset{\sim}{k})$, consider an exponential charge distribution,

$$\rho(\underset{\sim}{x}) = e^{-\Lambda|\underset{\sim}{x}|}\Lambda^3/(8\pi) \quad ,$$

$$\rho(\underset{\sim}{q}) = \Lambda^4/(q^2 + \Lambda^2)^2 \quad . \tag{3.24}$$

In Eq. (3.24), $\Lambda = 2/R$ in terms of the mean inverse radius $R = \langle r^{-1}\rangle^{-1}$. The rms radius $R_{rms} = \sqrt{3}\,R$ for this distribution. With Eq. (3.24), $\mathcal{F}(\underset{\sim}{k})$ may be evaluated via contour integration techniques as

$$\mathcal{F}(\underset{\sim}{k}) = \frac{2}{\pi}\tan^{-1}\frac{1}{kR} - \frac{1}{\pi}\,\frac{kR}{1 + (kR)^2} \quad . \tag{3.25}$$

Eq. (3.25) demonstrates explicitely that for $k < 1/R$, quantum effects are important. Unlike the classical expression in Eq. (2.8) for $\underset{\sim}{k}_1 = \underset{\sim}{0}$, which diverges as k^{-2} as $k \to 0$, Eq. (3.17) diverges only as k^{-1}. Of course, this remaining divergence is related to the use of first order perturbation theory, as is seen by comparing Eq. (3.20) with $1 \mp \delta D(k)$. This particular illness of perturbation theory can be compensated for by replacing $1 \mp \delta D$ by $G(\pm\delta D/\pi)$, which is correct to first order in $Z\alpha$, but also has the pleasant property of being exact for a point source. We will thus treat $\pm\delta D/\pi$ as the effective η parameter in the Gamow factor in Eq. (3.20). Since for $k \ll 1/R$ the exact distortion factor must reduce to $G(\eta)$, and $\pm\delta D/\pi \to \eta$ in that region, while for $k > 1/R$, $\delta D \ll 1$, replacing $1 \mp \delta D$ by $G(\pm\delta D/\pi)$ is very sensible and at the same time eliminates unphysical singularities arising in perturbation theory. Therefore, we replace Eq. (3.13) by

$$\sigma_{\pm}(k) = \sigma_0(k \mp \delta p(k))\; G\left(\pm \frac{\delta D(k)}{\pi}\right) \quad . \tag{3.26}$$

Furthermore, we stress that the exact form of $\mathfrak{F}(\underset{\sim}{k})$ is not crucial. The only important properties of $\mathfrak{F}$ are Eqs. (3.19) and (3.23). For most applications Eq. (3.25) will provide an adequate interpolation formula between the low and high k regions.

As an aside, we note that for nonspherical charge densities, Eq. (3.22) still holds. The peculiar angular dependence of the line integral is easily computed in the case of a uniform ellipsoid with major (minor) axis radii $R_Z(R_\perp)$. Then

$$4\pi \int_0^\infty d\tau \;\; \tau\rho(\hat{\underset{\sim}{k}}\tau) = \frac{3}{2} \; \frac{R_Z}{R_Z^2\sin^2\theta + R_\perp^2\cos^2\theta} \quad , \tag{3.27}$$

where $\cos\theta = \hat{\underset{\sim}{k}}\cdot\hat{\underset{\sim}{z}}$. The form factor $\mathfrak{F}(k,\theta)$ for large k is thus $(R_\perp/R_Z)^2$ smaller for $\theta = 90°$ than for $\theta = 0°$. In general, Coulomb distortions are largest for $\hat{\underset{\sim}{k}}$ along the largest linear dimensions of $\rho(\underset{\sim}{x})$ for a particle produced at $\underset{\sim}{x} = \underset{\sim}{0}$.

Next we calculate the impulse, $\delta p_\nu(k)$, for this static model. Since $j_\mu(\underset{\sim}{q},q_0) = \delta_{\mu 0}\, 2\pi\delta(q_0)\, \rho(\underset{\sim}{q})$, the energy impulse vanishes, $\delta p_0 = 0$. However, the vector momentum impulse in direction $\hat{\underset{\sim}{n}}$ is given by

$$\hat{\underset{\sim}{n}}\cdot\delta\underset{\sim}{p}(\underset{\sim}{k}) = 4\pi Z\alpha \mathrm{Re} \int \frac{d^3q}{(2\pi)^3} \; \frac{\underset{\sim}{q}\cdot\hat{\underset{\sim}{n}}}{2\underset{\sim}{k}\cdot\underset{\sim}{q} + q^2 - i\epsilon} \; \frac{2\omega_k \rho(-\underset{\sim}{q})}{q^2 - i\epsilon} \quad . \tag{3.28}$$

For $k \to 0$, it is convenient, as in Eq. (3.18), to change variables to $\underset{\sim}{p} = \underset{\sim}{q}/|\underset{\sim}{k}|$ and use $\rho(\underset{\sim}{q} = \underset{\sim}{0}) = 1$ to obtain

$$\hat{\underset{\sim}{n}} \cdot \delta\underset{\sim}{p}(\underset{\sim}{k}) \underset{\substack{\underset{\sim}{k} \to \underset{\sim}{0}}}{\longrightarrow} \frac{Z\alpha m_\pi}{\pi^2} \mathrm{Re} \int d^3p \, \frac{\underset{\sim}{p} \cdot \hat{\underset{\sim}{n}}}{2\underset{\sim}{p} \cdot \hat{\underset{\sim}{k}} + p^2 - i\epsilon} \frac{1}{p^2 - i\epsilon} \tag{3.29}$$

By symmetry, only the component of $\delta\underset{\sim}{p}$ along $\hat{\underset{\sim}{k}}$ could survive. However, even that component vanishes in the $\underset{\sim}{k} \to \underset{\sim}{0}$ limit:

$$\hat{\underset{\sim}{k}} \cdot \delta\underset{\sim}{p}(\underset{\sim}{k}) \underset{\substack{\underset{\sim}{k} \to \underset{\sim}{0}}}{\longrightarrow} \frac{2Z\alpha m_\pi}{\pi} \int_0^\infty dp \left\{ 1 - \frac{p}{4} \log \left| \frac{p+2}{p-2} \right| \right\}$$

$$= 0 \tag{3.30}$$

as verified by direct integration.

On the other hand, for $k \to \infty$, we proceed as in Eqs. (3.21) and (3.22) to obtain

$$\hat{\underset{\sim}{n}} \cdot \delta\underset{\sim}{p}(\underset{\sim}{k}) \underset{k \to \infty}{\longrightarrow} \mathrm{Re} \int_0^\infty d\tau \int \frac{d^3q}{(2\pi)^3} e^{-i2\underset{\sim}{k} \cdot \underset{\sim}{q}\tau} (2i\underset{\sim}{q} \cdot \hat{\underset{\sim}{n}}) \, \omega_k A_0(-\underset{\sim}{q}) |e|$$

$$= -\omega_k \int_0^\infty \frac{d\tau}{\tau} (\hat{\underset{\sim}{n}} \cdot \underset{\sim}{\nabla}_k) |e| A_0(\underset{\sim}{x} = 2\underset{\sim}{k}\tau)$$

$$= \frac{|e|}{\beta_k} \int_0^\infty d\tau \, \hat{\underset{\sim}{n}} \cdot \underset{\sim}{E}(\underset{\sim}{x} = \hat{\underset{\sim}{k}}\tau) \tag{3.31}$$

where we again changed variables in the last line, and $\underset{\sim}{E} = -\underset{\sim}{\nabla} A_0(\underset{\sim}{x})$ is the electric field for the static charge density along the straight-line trajectory $\underset{\sim}{x} = \hat{\underset{\sim}{k}}\tau$. Equation (3.31) is exactly what we would

obtain classically for the momentum impulse in the high momentum limit by integrating the relativistic Newton's equations.

A particularly important case of Eq. (3.31) is the component of $\delta\underset{\sim}{p}$ along $\underset{\sim}{k}$, i.e., $\hat{\underset{\sim}{n}} = \hat{\underset{\sim}{k}}$. For spherically symmetric densities this is clearly the only component $\delta\underset{\sim}{p}$. This impulse is given asymptotically by

$$\hat{\underset{\sim}{k}}\cdot\delta\underset{\sim}{p}(\underset{\sim}{k}) \underset{k\to\infty}{\longrightarrow} \frac{-1}{\beta_k}\,\mathrm{Re}\int_0^\infty d\tau\,\frac{d}{d\tau}\,A_0(\underset{\sim}{x} = 2\underset{\sim}{k}\tau)\;|e|$$

$$= A_0(\underset{\sim}{x} = 0)|e|/\beta_k \qquad (3.32)$$

Note that $|e|\,A_0(0)$ is simply the potential energy of the particle at the point of creation, and we recover Eq. (2.6) for $\underset{\sim}{k}_1 = \underset{\sim}{0}$ with β_k replacing k/m.

As an example of the complete form of $\delta\underset{\sim}{p}$, consider again the exponential distribution in Eq. (3.24). Evaluating Eq. (3.28) via residues gives

$$\delta\underset{\sim}{p}(\underset{\sim}{k}) = \hat{\underset{\sim}{k}}\;Z\alpha\;\omega_k\;\frac{kR}{1 + (kR)^2} \quad , \qquad (3.33)$$

where $R = \langle 1/r\rangle^{-1}$ is the mean inverse radius of the charge density. Equation (3.33) satisfies, of course, the required asymptotic forms Eq. (3.30) and (3.32). Note that unlike in the classical limit, Eq. (2.6), $|\delta\underset{\sim}{p}|$ is bounded by $|\delta\underset{\sim}{p}| \lesssim Z\alpha m_\pi$, for typical nuclear R, for all k. This boundedness of $\delta\underset{\sim}{p}$ is due to quantum effects. As with Eq. (3.25), Eq. (3.33) will be used from now on as a simple interpolation formula between the $k = 0$ and ∞ limits.

C. Non-Static Effects

Having obtained expressions for $\delta D(k)$ and $\delta p_\nu(k)$ for static charge densities, we turn now to study nonstatic effects.

For a charge density, $\rho(\underset{\sim}{x})$, moving uniformly with velocity $\underset{\sim}{v}_0$, the four current is obtained via a Lorentz transformation, $\Lambda_{\mu\nu}(\underset{\sim}{v}_0)$, as

$$j_\mu(x) = \Lambda_{\mu 0}\rho(\Lambda^{-1}x) \quad . \tag{3.34}$$

Since $\delta D(k)$ in Eq. (3.14) is a Loretz scalar and $\delta p_\nu(k)$ in Eq. (3.15) is a Lorentz vector, we could calculate the distortion factor and impulse for Eq. (3.34) using this Lorentz tranformation.

However, it is far simpler to recast the expressions obtained for the static charge densities in manifestly covariant form. For this purpose, it is convenient to define the four velocity u_μ of the charge density as

$$u_\mu = \Lambda_{\mu 0}(\underset{\sim}{v}_0) = (\gamma_0, \gamma_0\underset{\sim}{\beta}_0) \quad , \tag{3.35}$$

where $\underset{\sim}{\beta}_0 = \underset{\sim}{v}_0/c$ and $\gamma_0 = (1 - \beta_0^2)^{-1/2}$. In the rest frame of the charge density, $u_\mu = (1,\underset{\sim}{0})$. To construct the covariant expression, we need only note that if $\underset{\sim}{v}_0 = 0$, then $\omega_k = (ku)$, $|\underset{\sim}{k}| = ((ku)^2 - m^2)^{1/2}$ and $(0,\underset{\sim}{k}) = k - (ku)u$. Then the covariant form of δD from Eq. (3.17) is

$$\delta D(k) = \pi Z\alpha \frac{(ku)}{\left((ku)^2 - m^2\right)^{1/2}} \mathfrak{F}\left(\left((ku)^2 - m^2\right)^{1/2}\right) \tag{3.36}$$

The covariant impulse from Eq. (3.33) is

$$\delta p_\mu(k) = Z\alpha(k_\mu - (ku)\, u_\mu) \frac{(ku)R}{1 + \left((ku)^2 - m^2\right)R^2} \quad . \tag{3.37}$$

It is now straightforward to generalize Eqs. (3.36) and (3.37) to the case when $j_\mu(x)$ describes several independently moving charge densities carrying fraction f_i of the total charge Z, and with four velocities, u_i, and mean inverse radii, R_i. In this case,

$$\delta D(k) = \pi Z\alpha \sum_i f_i \frac{\omega_i'}{k_i'} \mathfrak{F}\left(k_i'\right) \quad , \tag{3.38}$$

and

$$\delta p_\mu(k) = Z\alpha \sum_i f_i (k - \omega_i' u_i)_\mu \frac{\omega_i' R_i}{1 + \left(k_i' R_i\right)^2} \quad , \tag{3.39}$$

where the energy in rest frame of charge density i has been denoted by

$$\omega_i' \equiv \left(ku_i\right) \quad , \tag{3.40}$$

and the magnitude of the three momentum in frame i has been denoted by

$$k_i' \equiv \left((ku_i)^2 - m^2\right)^{1/2} \quad . \tag{3.41}$$

Equations (3.38) through (3.41) describe Coulomb distortions generated by an arbitrary number of independently moving static charge fragments. For nuclear collisions, these charged fragments are the projectile and target fragments and the fireball. However, in addition to their relative motion, each of these sources has some internal excitation energy that will lead them to expand or evaporate in time. We must therefore also incorporate the non-static effect due to such expansions.

For nuclear collisions, the expansion velocities in the fireball rest frame are nonrelativistic ($v_T < 0.3c$). Therefore, Eq. (2.10) can be taken to describe the charge density in the fireball rest frame. The fireball distortion factor can then be calculated as in Eq. (2.12)

$$\delta D_f(k) = \int d^3v_0 \; f(\underset{\sim}{v}_0) \; \delta D(\Lambda^{-1}(\underset{\sim}{v}_0)k)$$

$$\approx \pi Z_f \alpha \frac{\langle \omega'_k \rangle_T}{\langle k' \rangle_T} \mathfrak{F}(\langle k' \rangle_T) \quad , \tag{3.42}$$

where we approximated the integral by evaluating δD at a mean thermal value of the relative energy and momentum. To determine the best choice of $\langle \omega'_k \rangle_T$ and $\langle k' \rangle_T$, note from Eq. (2.11) and (2.12) that thermal averaging is important only for low relative momenta, $k < k_T$. The main effect of the thermal averaging is to reduce the magnitude of δD for $k \gtrsim 0$. We will therefore choose $\langle \omega'_k \rangle_T$ and $\langle k' \rangle_T$ such that the $k \gtrsim 0$ limit is correctly given by the approximate form in Eq. (3.42).

If the velocities $\underset{\sim}{v}_o$ are so low that the Lorentz boosted relative momentum, $\langle k' \rangle_T$, in Eq. (3.42) is small compared to 1/R as $|\underset{\sim}{k}| \to 0$, then $\overset{\sim}{\mathcal{J}} \approx 1$ and

$$\delta D_f(k) \underset{k\to o}{\longrightarrow} \pi Z_f^{\alpha} \int d^3 v_o \frac{f(\underset{\sim}{v}_o)}{v_o} = \frac{\pi Z_f^{\alpha}}{\beta_T} \quad , \tag{3.43}$$

where $\beta_T = \langle 1/\beta \rangle^{-1}$ is the mean inverse thermal velocity. Comparing to Eq. (3.42), we see that we should chose $\langle \omega_k' \rangle_T$ and $\langle k' \rangle_T$ such that $\langle k' \rangle_T / \langle \omega_k' \rangle_T \to \beta_T$ as $k \to o$. The mean Lorentz boosted relative energy, $\langle \omega_k' \rangle_T$, is of the form $\langle \gamma_o(\omega_k + \underset{\sim}{\beta}_o \cdot \underset{\sim}{k}) \rangle_T = \gamma_T \omega_k$ in terms of the observed particle energy. Note that we used $\langle \underset{\sim}{\beta}_o \rangle_T = 0$ for thermal $f(\underset{\sim}{v}_o) = f(-\underset{\sim}{v}_o)$, and γ_T is the mean Lorentz boost γ factor. The mean magnitude of the momentum $\langle k' \rangle_T$ is then approximately related to $\langle \omega_k' \rangle_T$ via $\langle k' \rangle_T = (\langle \omega_k' \rangle_T^2 - m^2)^{1/2} \to (\gamma_T^2 - 1)^{1/2} m$ as $k \to 0$. Therefore, if we chose $\gamma_T = (1-\beta_T^2)^{-1/2}$, then the approximate form in Eq. (3.42) reduces to the correct limit as $|\underset{\sim}{k}| \to 0$. For a Boltzmann distribution of protons at a temperature T, $\beta_T = ((\pi/2)T/m_p)^{1/2}$ and this prescription leads to

$$\gamma_T = \left(1 - (\pi/2)\ T/m_p\right)^{-1/2} \quad . \tag{3.44}$$

The fireball distortion factor is thus

$$\delta D_f(k) \approx \pi Z_f^{\alpha} \frac{\gamma_T(\omega_k)}{\left(\gamma_T^2(\omega_k)^2 - m^2\right)^{1/2}} \mathcal{F}\left(\left(\gamma_T^2 \omega_k^2 - m^2\right)^{1/2}\right)$$

$$= \pi Z_f^{\alpha} \frac{\gamma_T(ku_F)}{\left(\gamma_T^2(ku_F)^2 - m^2\right)^{1/2}} \mathcal{F}\left(\left(\gamma_T^2(ku_F)^2 - m^2\right)^{1/2}\right) \quad , \tag{3.45}$$

where in the last line we have expressed δD_f in covariant form by introducing the fireball center of mass four velocity u_F.

Comparing eq. (3.45) to Eq. (3.36), we see that thermal averaging can be simply approximated by replacing (ku) by $\gamma_T(ku)$ where γ_T is given by Eq. (3.44). Therefore, the Coulomb distortion and impulse for several independently moving fireballs with temperatures T_i is given by Eqs. (3.38) and (3.39), where the relative energy and momentum in the rest frame of fireball i are now given by

$$\omega_i' = \gamma_{T_i}(ku_i) \quad , \tag{3.46}$$

$$k_i' = (\omega_i'^2 - m^2)^{1/2} \quad . \tag{3.47}$$

Equations (3.38), (3.39), (3.46) and (3.47) specify the ingredients necessary to calculate Coulomb distorted cross sections for nuclear collisions via Eq. (3.26). In the next section we apply these formulas to recent pion and nucleon inclusive data.

IV. Applications

A. Coulomb Distorted Fireball Model

As a working model for the charge, velocity, and temperature distributions as well as the inclusive cross sections in nuclear collisions, we will use the fireball model.[9] For a given impact parameter b, the number of participant $N_F(b)$ and spectator, $N_{P'}(b) + N_{T'}(b)$, nucleons are determined using straight line geometries. The charge carried by the projectile and target fragments are then $(Z_P/A_P)\ N_{P'}(b)$ and $(Z_T/A_T)\ N_{T'}(b)$, where Z_P, A_P, Z_T, A_T are the initial projectile and target charge and nucleon numbers. The charge on the fireball is given by

$$Z_F(b) = \frac{Z_P}{A_P}\ (A_P - N_{P'}) + \frac{Z_T}{A_T}\ (A_T - N_{T'}) \quad . \tag{4.1}$$

The fireball velocity and excitation energy per nucleon, $E^*(b)$, are determined by energy-momentum conservation.[9] Cooling due to pion production is taken into account via Kapusta's formula[9]

$$T_F(b) = T_0[1 - \exp(-2E^*(b)/3T_0)] \quad , \tag{4.2}$$

with $T_0 \sim 100$ MeV. The projectile and target fragments are given 8 MeV of temperature unless otherwise specified, in accord with observations from projectile fragmentation studies. From energy-momentum conservation, this small internal excitation energy requires that the projectile fragment slows down by $\Delta v \sim (3T/2M_N)\ v_0$ and the target fragment speeds up by $\sim\Delta v$, where $T \approx 8$ MeV and v_0 is the projectile velocity.

The radii, R_i, in Eqs. (3.38, 3.39) are taken as the rms radii, $R_i = 1.2N_i^{1/3}$ fm, corresponding to normal nuclear density. We deliberately use the rms rather than the mean inverse radii because the observed particle at the freezout time, $t = 0$, is most likely found at a radius $|\underset{\sim}{x}| \approx R_{rms}$ rather than $|\underset{\sim}{x}| = 0$. Thus, the initial potential energy of the particle (see Eq. (3.32)) is $\approx Z\alpha/R_{rms}$, which is significantly smaller than the potential at the origin, $Z\alpha\langle 1/r\rangle$. We also consider 20 percent variations of this rms radius to test for sensitivity of results to initial conditions.

Finally, for the neutrals cross section in the fireball rest frame, we take

$$\sigma_o(\underset{\sim}{k},b) \propto \omega_k \exp[-\omega_k/T_F(b)] \quad , \tag{4.3}$$

with $\omega_k = (k^2 + m^2)^{1/2}$. For impact parameter averaged cross sections we approximate by calculating with $b = b^*$, the most probable impact parameter, which maximizes $b^2 N_F(b)$.

Note that in computing Coulomb effects via Eq. (3.26), we need in principle to specify the off-shell form of $\sigma_o(\underset{\sim}{k}_o,\underset{\sim}{k})$ for $k_o \neq \sqrt{k^2 + m^2}$. This is because relativistic quantum effects in Eq. (3.37) can lead to $\delta P_o \neq o$. However, in the spirit of the fireball model, where all particles are assumed to be on-shell, we will neglect any off-shell k_o dependence of σ_o. This is done by replacing k_o by ω_k in the fireball frame, as in Eq. (4.3). Therefore, only the <u>three</u> momentum shift, $\delta\underset{\sim}{p}(\underset{\sim}{k})$, calculated in the fireball frame, will be considered here.

B. π^-/π^+ Ratio

The first application of our formulas will be to the Benenson et al.[1] data on the π^-/π^+ ratio for $\theta_{Lab} = 0^\circ$. The main features we want to explain are (1) the sharp peak near the projectile rapidity, y_p, (2) the asymmetry of the ratio for $y < y_p$ and $y > y_p$, and (3) the monotonic decrease of π^-/π^+ at large $y >> y_p$ as a function of decreasing bombarding energy.

Figure I displays the data for Ne + NaF $\rightarrow \pi^\pm$ for (a) $E_{Beam} = 383$ and (b) 164 MeV/nucleon. The rapidity of the incident beam is indicated by the symbol B. The solid curves are the results of the Coulomb distorted fireball model. The symbol F locates the rapidity of the fireball, P' locates the rapidity of the excited projectile fragment, and T' locates the rapidity of the excited target fragment.

With Eqs. (4.3) and (3.26), the π^-/π^+ ratio for a given pion momentum $\underset{\sim}{k}$ in the fireball frame is given by

$$\frac{\pi^-(\underset{\sim}{k})}{\pi^+(\underset{\sim}{k})} = \left\{\frac{\omega_k^-}{\omega_k^+} e^{-(\omega_k^- - \omega_k^+)/T_F}\right\} e^{2\delta D(k)} , \qquad (4.4)$$

where $\omega_k^\pm = ((\underset{\sim}{k} \mp \delta\underset{\sim}{p}(\underset{\sim}{k}))^2 + m_\pi^2)^{1/2}$, and the three momentum $\delta\underset{\sim}{p}(\underset{\sim}{k})$ and $\delta D(\underset{\sim}{k})$ are calculated from Eqs. (3.38), (3.39), (3.46) and (3.47) using the values of the four velocities u_i and k in the fireball frame. In Eq. (4.4) we have explicitly neglected possible off-shell effects through $\delta p_o(\underset{\sim}{k})$ as discussed below Eq. (4.3). For $\underset{\sim}{k}$ corresponding to the velocity of the projectile (in the fireball frame), the projectile fragment contribution to $\delta D(\underset{\sim}{k})$ in Eq. (3.38) dominates, and $\delta D(\underset{\sim}{k}) \approx \pi Z_{p'\alpha}/\beta_{Tp'}$.

However, the projectile form factor and the contribution of the fireball and target remnant to δD lead to 20 percent corrections to this simple formula. Including all terms, we find that $\exp(2\delta D) \approx 10$ for the 383 MeV/nucleon case. The average impact parameter we use is $b^* = 3.42$ fm such that $Z_{p'} = Z_{T'} = 6.4$, $Z_F = 7.2$, $R_{p'} = R_{T'} = 2.8$ fm, $R_F = 2.9$ fm. On the other hand, near the projectile rapidity, the impulse is dominated by the target fragment and the fireball as seen from Eq. (3.39). Therefore, $\delta p \approx Z_{T'}\alpha/R_T + Z_F\alpha/R_F \approx 7$ MeV/c. The term in the brackets in Eq. (4.3) supresses the π^-/π^+ ratio due to this momentum shift by a factor $\exp(-6\ \text{MeV}/T_F)$. In the fireball model $T_F = 26.8$, 45.6 MeV for $E_{Beam} = 164$, 383 MeV/nucleon respectively. Thus, for 383 MeV/nucleon, $\pi^-/\pi^+(y = y_{p'}) \approx 0.9 \times 10 = 9$ as seen in Fig. Ia.

Note that because Ne + NaF is a symmetric system, the π^-/π^+ ratio is symmetric about the fireball rapidity y_F. Thus, our formulas also predict a peak at $y = y_{T'}$ identical to the one at $y = y_{p'}$. On the other hand, there is no peak at the fireball rapidity due to the high radial expansion velocity of the fireball. This expansion limits the fireball contribution to δD. Note also that the magnitude of the asymmetry above and below $y_{p'}$, due to the multiple charged fragments, is correctly predicted in our model.

To test the sensitivity of the results to the initial conditions, the initial radii were reduced by 20 percent. The dotted curve in Fig. Ia indicates that the peak height was thereby increased by ~20 percent. We note that the peak height has a complicated dependence on all the variables as seen via

$$\left(\frac{\pi^-}{\pi^+}\right)_{max} \approx \exp\left\{2\delta D(k^*) - 2\left(\frac{k^*}{\omega^*}\right)\frac{\delta p(k^*)}{T_F}\right\} \quad , \tag{4.5}$$

where k* is the pion momentum in the fireball frame corresponding to zero relative momentum in the projectile frame. Finally, the asymptotic value of π^-/π^+ for $y >> y_p$ is given by

$$\frac{\pi^-}{\pi^+} \xrightarrow[y>>y_{p'}]{} \exp\left\{-\frac{2}{T_F}\left(\frac{Z_{T'}\alpha}{R_{T'}} + \frac{Z_F\alpha}{R_F} + \frac{Z_{p'}\alpha}{R_{p'}}\right)\right\} \quad , \tag{4.6}$$

where we used $\omega^- - \omega^+ \to 2\delta p$ and $\delta D \to 0$ in this limit. This is similar to the formula obtained by Bertsch[2] except that we include the momentum shift due to the projectile and target fragments as well. While there is good quantitative agreement between the full calculation and data at $y \approx 1.4$, this asymptotic form has not yet been reached. Comparing Figs. I(a),(b), note also that the high y ratio is decreasing at lower beam energies because T_F is decreasing.

Finally, we show in Fig. II the angular dependence of the π^-/π^+ ratio for pion momentum $p_{lab} = 100$ MeV/c, below the projectile velocity, $p_{lab} = 130$, at the projectile velocity, and $p_{lab} = 160$, above the projectile velocity for the 383 MeV/nucleon case. As seen from Fig. II, the expected angular spread of the Coulomb effect is small, $\Delta\theta_{lab} \lesssim 10^\circ$. Thus the π^-/π^+ peak is sharply peaked in the forward direction.

We emphasize that the good agreement of our calculations with the data indicates that quantum effects are well described via the generalized Gamow factor in Eq. (3.26). In the region of the peak, perturbation theory cannot be used because $\delta D > 1$. Neither could a classical calculation[3] describe this long relative wavelength

regime. The non-perturbative extension via Eq. (3.26) provides a simple quantitative formula that is seen to describe this non-perturbative quantum region well.

C. π^+ Spectra and Coulomb Focusing

The second application of our formulas is to the π^+ inclusive data on Ne + NaF at 800 MeV/nucleon.[4] The π^+ invariant cross section is given from Eqs. (3.26) and (4.3) in the fireball frame by

$$\sigma_{\pi^+}(k) = \tilde{\sigma}\ \omega_k^+ e^{-\omega_k^+/T_F}\left\{\frac{2\delta D(k)}{e^{2\delta D(k)}-1}\right\} \quad , \tag{4.7}$$

with ω_k^+ being the shifted π^+ energy as given below Eq. (4.4), and $\delta\underset{\sim}{p}(\underset{\sim}{k})$ and $\delta D(\underset{\sim}{k})$ are determined as before. The normalization constant $\tilde{\sigma}$ is chosen by fitting the peak value of the π^+ data[4] at $\theta_{cm} = 90^\circ$ and $p_\perp = 60$ MeV/c.

Figure IIIa shows the contour plot of the generalized Gamow factor, the bracketed term in Eq. (4.7). The charge distribution of the three charged fragments for this reaction is characterized by the following parameters: $Z_{p'} = Z_{T'} = 6.4$, $Z_F = 7.2$, $R_{p'} = R_{T'} = 2.8$ fm, $R_F = 2.9$ fm, $b^* = 3.42$ fm, $N_F(b) = 14.3$, $T_{p'} = T_{T'} = 8$ MeV, $T_f = 67.4$ MeV, $y_{p'} - y_F = y_F - y_{T'} = 0.59$. From Fig. IIIa, this phase space factor is seen to reach a minimum at the rapidity of the projectile and target fragment. That value is 0.28. At the fireball rapidity, the phase space suppression is 0.68. For larger $p_\perp$, this factor approaches unity.

In Fig. IIIb, the π° invariant cross section, σ_{π° is plotted in units of barns/(sr·GeV^2) in this fireball model. The σ_{π° is peaked at $y = y_F = 0$ and $p_\perp = 0$ and is isotropic in the fireball frame. In Fig. IIIc, $\sigma_{\pi^+}(k)$ from Eq. (4.7) is shown in the same units. We observe that as a result of the large phase space suppression for $p_\perp < 30$ MeV/c in Fig. IIIa, the π^+ spectra peaks broadly at finite $p_\perp \sim 60$ MeV/c. Near the projectile and target rapidities there is a substantial suppression of the π^+ yield as compared to the π° yield in accord with the results of section IV.B. Comparing to the data[4] in Fig. IV(a), we see that the magnitude and location of the broad peak is in good qualitative agreement with the observed spectra in the mid rapidity region.

We have also varied the amount of charge in the three fragments by chosing different impact parameters. For b = 6.4 fm, $Z_{p'} = Z_{T'} = 10$, $Z_F = 0$, corresponding to perfect transparency, we find as in Fig. I of Ref. 3 that this charge distribution only leads to a ridge at $y = 0$ peaked at $p_\perp = 0$. For very central collisions or high opacity, we studied b = 2.12 fm, for which $Z_{p'} = Z_{T'} = 3.8$ and $Z_F = 12.4$. In that case the phase space suppression at $y = y_{p'} = y_T$ was 0.45, a substantial change from 0.28 in Fig. IIIa. However, the suppression at $y = y_F$ and $p_\perp = 0$ was 0.64, a value very close to 0.68 in Fig. IIIa. Thus, while the projectile and target rapidity regions were strongly affected by this variation in the charge density, the mid rapidity fireball region was insensitive to this variation. This insensitivity of the mid rapidity region to increasing the fireball charge is due largely to

the high expansion velocity of the fireball that limits the fireball contribution to δD. The projectile and target rapidity regions are, on the other hand, quite sensitive to charge variations because of the much lower excitation energies ($T \lesssim 8$ MeV).

From these studies it is clear that the high thermal expansion velocity of the fireball must be incorporated in calculating Coulomb effects. The greater sensitivity to the mid rapidity charge distribution via the parameter α in Ref. 3 is due to the neglect of this expansion rate. This point is mentioned but not emphasized in Ref. 3.

Next, we discuss the sensitivity of the π^+ bump structure to the production model, Eq. (4.3). In particular, consider the width of the bump as a function of rapidity at $p_\perp = 60$ MeV/c as defined by the $\sigma_{\pi^+} = 1.4$ contour line in Fig. IIIc. The total rapidity width of this contour is $\Delta y \sim 0.6$. Comparing with Fig. IIIb, it is clear that this width is simply a reflection of the width of the thermal distribution at $p_\perp = 60$ MeV/c. Therefore, the precise form of the bump depends the production model quite sensitively. To emphasize this point more clearly consider the difference between the π^+ spectra at 400 MeV/nucleon and 800 Mev/nucleon in fig. IV. While at 800 MeV/nucleon, Fig. IVa, there exists a bump structure, no such bump is observed at the lower energy. This is a key observation of Ref. 4.

If we apply the fireball model to the lower energy data, then the predicted π^+ spectra is found to have almost the same bump structure as in Fig. IIIc. The only way we can account for the absence of the bump at lower energies is that the clearly visable and non-isotropic Δ_{33} resonance decay dominates the production dynamics. Therefore, for a fixed $p_\perp \approx 75$ MeV/c the cross section has a minimum at $y = y_F$ in contrast to a maximum that is always found in an isotropic fireball distribution. The crucial point is that Coulomb distortions lead to a bump at $y = y_F$, $p_\perp \neq 0$ only if the undistorted π° cross section has a maximum at $y = y_F$! In the 400 MeV/nucleon data this condition is clearly not satisfied. The only effect of Coulomb distortions in this case is to suppress the low $p_\perp \lesssim 30$ MeV/c π^+ yield. At 800 MeV/nucleon, the fireball contribution to the π^+ yield can be disentangled from the Δ contribution. Thus, the condition for the creation of a bump is satisfied.

For the Ar + Ca system[5] studied in Ref. (3), the fireball contribution is also visable, and hence Coulomb distortions lead to a bump at finite $p_\perp$. Our calculations for this reaction are qualitatively similar to those of Ref. 3. However, the V structure of the bump is not reproduced in the fireball model. We do find, though, very little sensitivity of the bump structure to variations in the charge distribution, i.e., insensitivity to b^*, which was also found in the Ne + NaF case. Again this insensitivity is due to the high expansion velocity of the fireball. For a quantitative explanation of the bump structure a much better model for the production dynamics is required.

We conclude by emphasizing that Coulomb distortions lead to a bump structure under the condition that $\sigma_{\pi^0}(y,p_\perp)$ has a maximum at $y = y_F$ for fixed $p_\perp$. Furthermore, the details of that structure are determined mainly by the production dynamics and not Coulomb final state interactions.

D. The n/p ratio

The calculation of the Coulomb effects on the n/p ratio for Ne+U is complicated by the following factors: 1) the initial n/p ratio in the projectile and target differ greatly, $(n/p)_{Ne} = 1.0$, $(n/p)_U = 1.6$, 2) composite fragment production plays a major role in the reaction with up to 2/3 of the protons with energy >20 MeV ending up in light composites,[10,11] 3) the neutrons and protons are measured in separate experiments at different beam energies, 4) for nucleons with lab energy $\leq$30 MeV, the target remnant evaporation products compete in yield with the mid rapidity fireball products. All four of these factors lead to a complex angular and energy dependence of the n/p ratio even without Coulomb effects. It is clear that for a quantitative comparison with data a rather sophisticated calculation is necessary.

Since our purpose here is to gain insight into the qualitative effects due to Coulomb final state interactions, we will continue to study the naive fireball model. However, to include the qualitative effect of composite formation on the n/p ratio, we follow the method proposed by Stock:[10] If N, Z are the total neutron and proton numbers in the fireball and if Z_B is the total number protons bound

in isospin I = 0 composites, then $N - Z_B$ and $Z - Z_B$ are the final number of free neutrons and protons. These free nucleons are then distributed in the fireball frame as

$$\sigma_n(\underset{\sim}{k}) = \bar{\sigma}(N-Z_B)\,\frac{1}{T^{3/2}}\exp\left(-\frac{k^2}{2m_N T}\right) \quad , \tag{4.8}$$

$$\sigma_p(k) = \bar{\sigma}(Z-Z_B)\,\frac{1}{T^{3/2}}\exp\left\{-\frac{(\underset{\sim}{k}-\delta\underset{\sim}{p}(k))^2}{2m_N T}\right\} G\left(\frac{\delta D(k)}{\pi}\right) \quad , \tag{4.9}$$

where $G(\delta D/\pi)$ is the generalized Gamow factor as in Eq. (4.7), and $\delta\underset{\sim}{p}$ and δD are computed as before. To take into account the different beam energies for the neutrons and protons, the temperature in Eqs. (4.8) and (4.9) must differ. For Ne+U→n+x at 337 MeV/nucleon,[8] T = 37.8 MeV, while for Ne+U→p+x at 393 MeV/nucleon[11] T = 42.2 MeV, in our model.

For the calculation of the Coulomb distortion we took $b^* = 6.2$ fm, $Z_F = 19$, $Z_{T'} = 80$, $Z_{p'} = 3$, $R_F = 4.2$, $R_{T'} = 7.1$, $R_{p'} = 2.2$ fm.

The n/p ratio calculated this way is shown in Fig. V for the case $Z_B = 0$, i.e., no composites. The dashed-dot curve shows n/p in the fireball model with Coulomb effects turned off. The energy dependence arises solely from the different temperatures for the neutrons and protons, and the magnitude is determined both by the N/Z = 1.36 ratio in the fireball and the temperature difference. The dashed curve shows the effect of the phase space distortions, $\delta D \neq 0$, for protons, but with no momentum shift, $\delta\underset{\sim}{p} = 0$. As seen from Fig. V, there is

an appreciable phase space distortion below 30 MeV in the lab. For example, for E_{lab} = 20 MeV, $\theta_{lab} = 30^{o}$, $G(\delta D/\pi) = 0.67$. Note that, the phase space suppression of protons is nearly isotropic, as $G(\delta D/\pi) = 0.70$ for 90^{o} at that same energy. This near isotropy of the Coulomb effects in the lab is due to the cold, high Z target remnant and to the fact that the fireball contribution is reduced due to the high expansion velocity.

The full curves show the n/p ratio with both δD and $\delta \underline{p}$ included. Comparing the dashed and solid curves, we see that the Coulomb momentum shift reduces the n/p ratio at high energies where the gradient of the cross section is the largest. Because the target remnant has the greatest effect, it is the gradients in the lab frame that matter the most. Thus the 90^{o} yield, which falls off much more rapidly than the 30^{o} yield in the lab frame, has the largest reduction of the n/p ratio due to this momentum shift. Above 100 MeV, the Coulomb distortions are dominated by $\delta \underline{p}$ and reduce n/p by a factor $\sim \exp(-Z_T\alpha/R_T T - Z_F\alpha/R_F T) \approx 0.6$.

While the data[8] are also shown in Fig. V for comparison, we cannot draw any conclusions at this stage about the apparent agreement or disagreement between the solid curve and the data. We have not adequately included into these calculations the many complex factors mentioned before. For example, from Ref. (11) it is known that up to 2/3 of the protons with $E_{lab} > 20$ MeV are bound in light composites. Thus, $Z_B/Z \sim 2/3$ in Eqs. (4.8), (4.9). With such a large Z_B, the n/p ratio is enhanced[10] by a factor $(N-Z_B)/(Z-Z_B) \times Z/N = 1.5$

relative to the case $Z_B = 0$ plotted in Fig. V. Including this effect would thus shift all calculated curves up uniformly by this factor in Fig. V. Therefore, composite fragment production affects the n/p ratio at least as much, if not more, than Coulomb distortions.

Our aim here was simply to calculate the magnitude of Coulomb effects. We find that distortions of the n/p ratio for Ne + U due to Coulomb final state interations alone are on the order of 50 percent, and hence cannot be neglected in future calculations.

VI. Concluding Remarks

With the formulas obtained in Section III, we have been able to provide analytical insight into several peculiar features of current data on nuclear collisions. The primary value of these formulas is in obtaining a quick estimate of the effect of Coulomb final state interactions for the complicated non-static charge currents arising in nuclear collisions. In particular, the regions of momentum phase space where Coulomb effects are important can be readily found. Our formulas also provide a natural bridge between the relativistic, quantum and classical domains. Thus, the π^-/π^+ data[1] at $y = y_p$, $p_\perp = 0$ and the π^+ data[4,5] at $y = y_F$, $p_\perp \sim m_\pi/2$ could be treated on the same footing.

One general conclusion is that the projectile and target fragmentation regions are much more sensitive to the actual charge distribution than is the mid-rapidity fireball region. We have shown that this is due to the high thermal expansion velocities of the participant (fireball) nucleons, as opposed to the much slower expansion velocities of the spectator (projectile and target fragment) nucleons. Thus, to use Coulomb effects to learn about the true charge current in nuclear collisions, it is more profitable to study the fragmentation regions. Furthermore, pions are a much cleaner probe of the charge current than the protons. This is because composite formation and target and projectile evaporation strongly affect the proton spectra.

Finally, we note that our formulas are easily generalized to treat Coulomb distortions of light composite spectra. A fruitful extension of our fireball calculations would be to incorporate the Coulomb phase space factor, δD, and the momentum shift, $\delta \underline{p}$, into the generalized firestreak model,[9] which includes composite formation.

Acknowledgements:

We are grateful to G. Westfall for use of his fireball geometry code. Useful discussions with S. K. Koonin, L. W. Wilson, W. Benenson, R. Stock, and G. Bertsch are also gratefully acknowledged. This work was supported by the Nuclear Physics Division of the U. S. Department of Energy under Contract No. W-7405-ENG-48.

References

1. W. Benenson, G. Bertsch, G. M. Crawley, E. Kashy, J. A. Nolan, Jr., H. Bowman, J. G. Ingersoll, J. O. Rasmussen, J. Sullivan, M. Koike, M. Sasao, J. Peter, T. E. Ward, Phys. Rev. Lett. 43 (1979) 683; and Errata, Phys. Rev. Lett. 44 (1980) 54.
2. G. Bertsch, Nature 283 (1980) 280.
3. K. G. Libbrecht, S. E. Koonin, Phys. Rev. Lett. 43 (1979) 1581.
4. J. Chiba, K. Nakai, I. Tannihata, S. Nagamiya, H. Bowman, J. Ingersoll, and J. O. Rasmussen, Phys. Rev. C20 (1979) 1332; K. Nakai, J. Chiba, I. Tannihata, M. Sasao, H. Bowman, S. Nagamiya, and J. O. Rasmussen, Phys. Rev. C20 (1979) 2210.
5. K. L. Wolf, H. H. Gutbrod, W. G. Meyer, A. M. Poskanzer, A. Sandoval, R. Stock, J. Gosset, C. H. King, G. King, Nguyen Van Sen, and G. D. Westfall, Phys. Rev. Lett. 42 (1979) 1448.
6. L. I. Schiff, Quantum Mechanics, Third Editor (McGraw-Hill, N. Y., 1968) 142.
7. M. Gyulassy, S. K. Kauffmann, and Lance W. Wilson, Phys. Rev. C20 (1979) 2267.
8. W. Schimmerling, J. W. Kast, D. Ortendahl, R. Madey, R. A. Cecil, B. D. Anderson, A. R. Baldwin, Phys. Rev. Lett. 43 (1979) 1985.
9. J. Gosset, J. I. Kapusta, G. D. Westfall, Phys. Rev. C18 (1978) 844, and references therein.
10. R. Stock and J. Stevenson, private communication.
11. S. Sandoval, H. H. Gutbrod, W. G. Meyer, A. M. Poskanzer, R. Stock, J. Gosset, J.-C. Jourdain, C. H. King, G. King, C. H. Lukner, Nguyen Van Sen, G. D. Westfall, K. L. Wolf, LBL-8771, preprint (1979).

Figure Captions:

I. The π^-/π^+ ratio at $\theta_{lab} = 0^o$ as a function of rapidity $y_{lab} = 1/2\ \ln|(1+v_\pi)/(1-v_\pi)|$. The reaction[1] is Ne+NaF$\rightarrow\pi^\pm$ at (a) 383 MeV/nucleon (square points) and (b) 164 MeV/nucleons (solid dots). Solid curve shows Coulomb distorted fireball model results, Eq. (4.4). Rapidities of the beam B, projectile fragment P', fireball F, and target fragment T' are indicated. Dotted segment in (a) shows sensitivity of results to 20 percent reduction of initial radii.

II. The expected angular distribution of the π^-/π^+ ratio for Ne + NaF$\rightarrow\pi^-/\pi^+$ at 383 MeV/nucleon for fixed pion lab momenta near the projectile rapidity region.

III. Contour plot as a function of $(y,p_\perp)$ of a) the generalized Gamow factor in Eq. (4.7), b) the π^o invariant cross section (barns/sr. GeV^2), and c) the π^+ invariant cross section, Eq. (4.7) for Ne + NaF$\rightarrow\pi^+$ at 800 MeV/nucleon.

IV. Contour plot[4] of measured invariant π^+ cross section for Ne + NaF at (a) 800 MeV/nucleon and (b) 400 MeV/nucleon. A useful gauge of the uncertainties of these contour lines can be obtained by comparing these plots to the published ones in Ref. (4) using the same data base.

V. The ratio of invariant neutron to proton cross section for Ne+U$\rightarrow$n+X at 337 MeV/nucleon[8] and Ne+U$\rightarrow$p+x at 393 MeV/nucleon.[11] The dashed-dot curve is the expected n/p ratio in the fireball model without Coulomb effects. The dashed curve

includes effects of the Coulomb phase space distortions $G(\delta D/\pi)$ in Eq. (4.9). The full curve includes also the Coulomb momentum shift δp in Eq. (4.9). These curves are for the case $Z_B = 0$, i.e., no composite production. In this model, Eqs. (4.8, 4.9), composite production shifts all curves up by a constant factor.

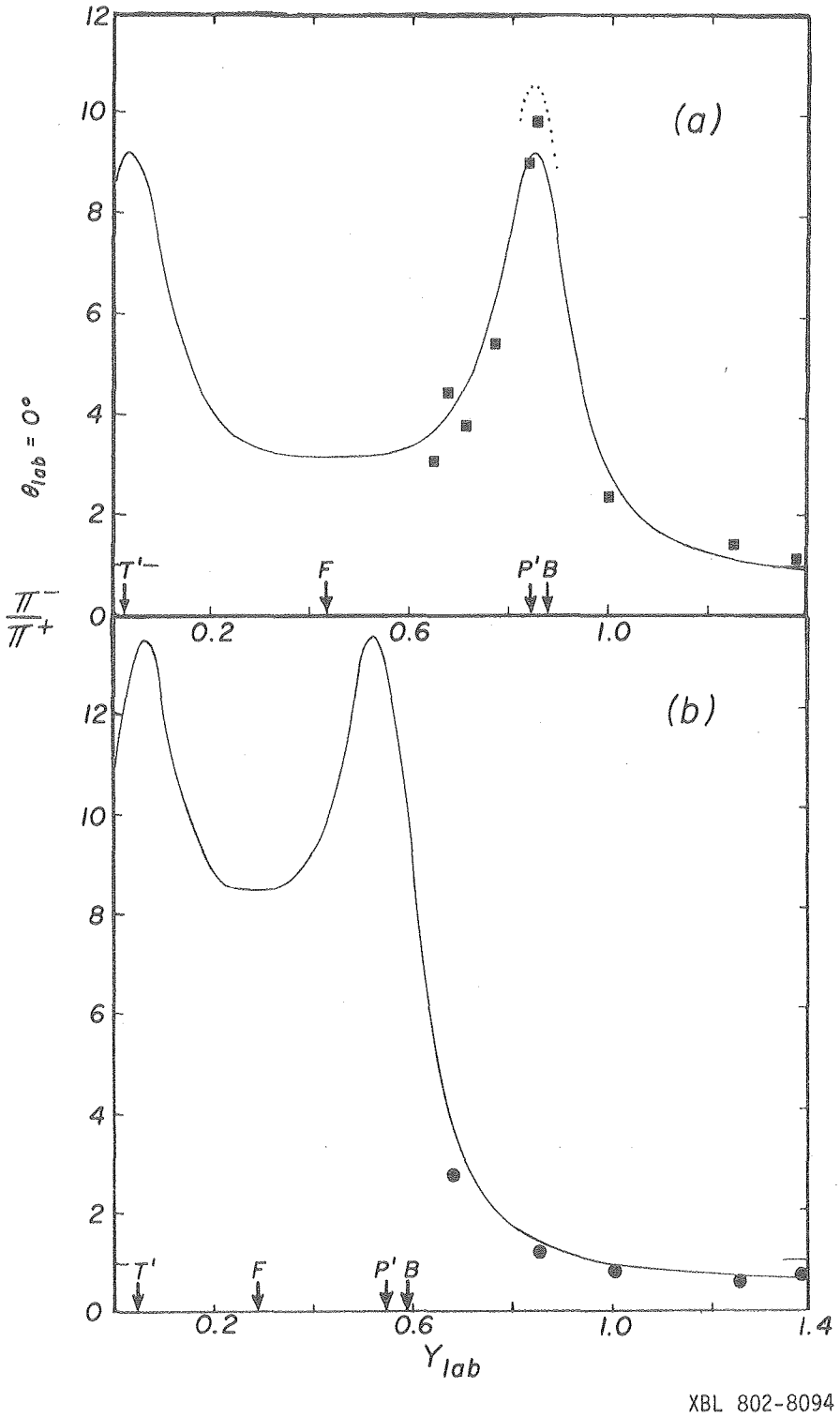

Fig.I

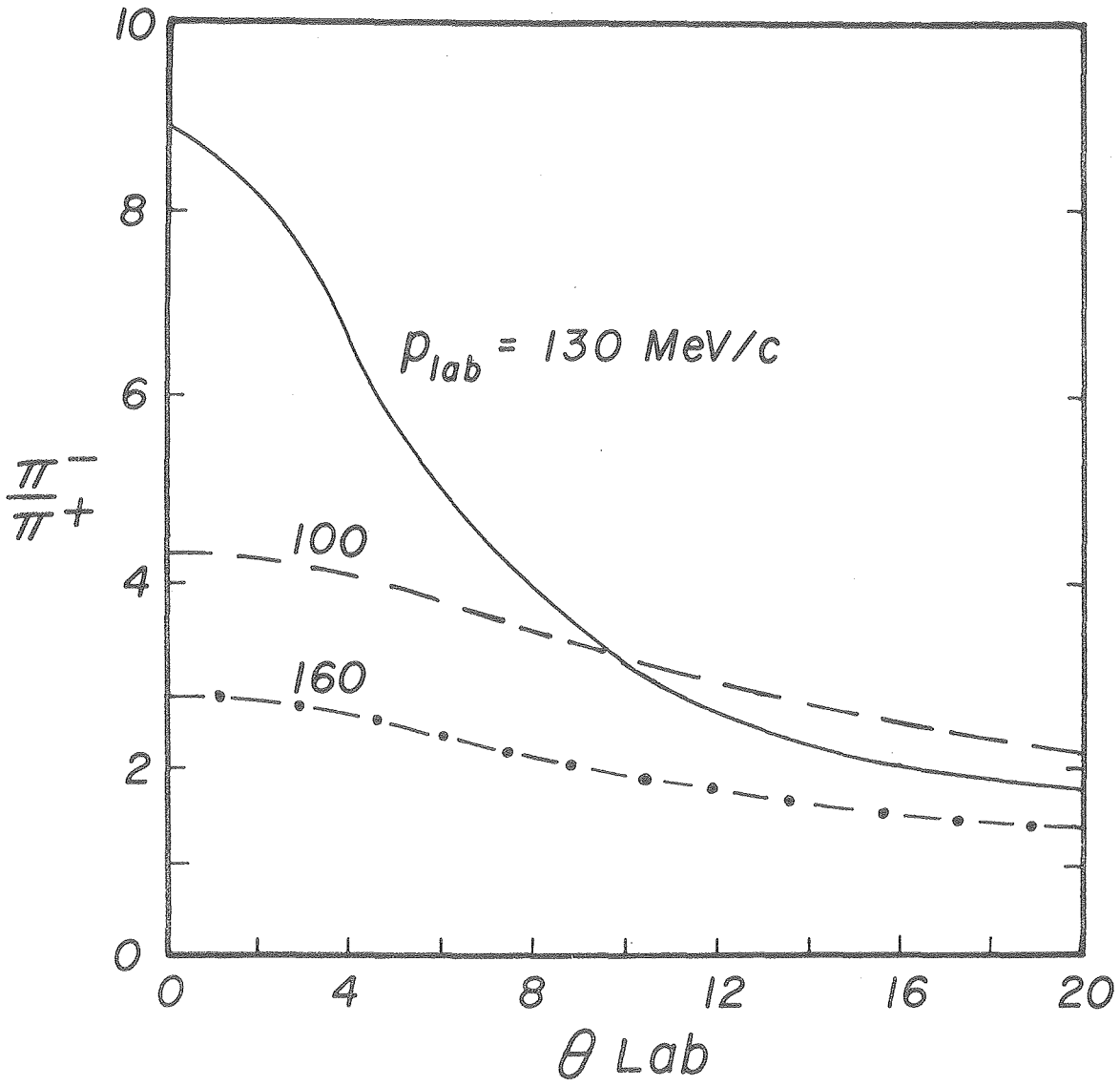

XBL 802-8093

Fig.II

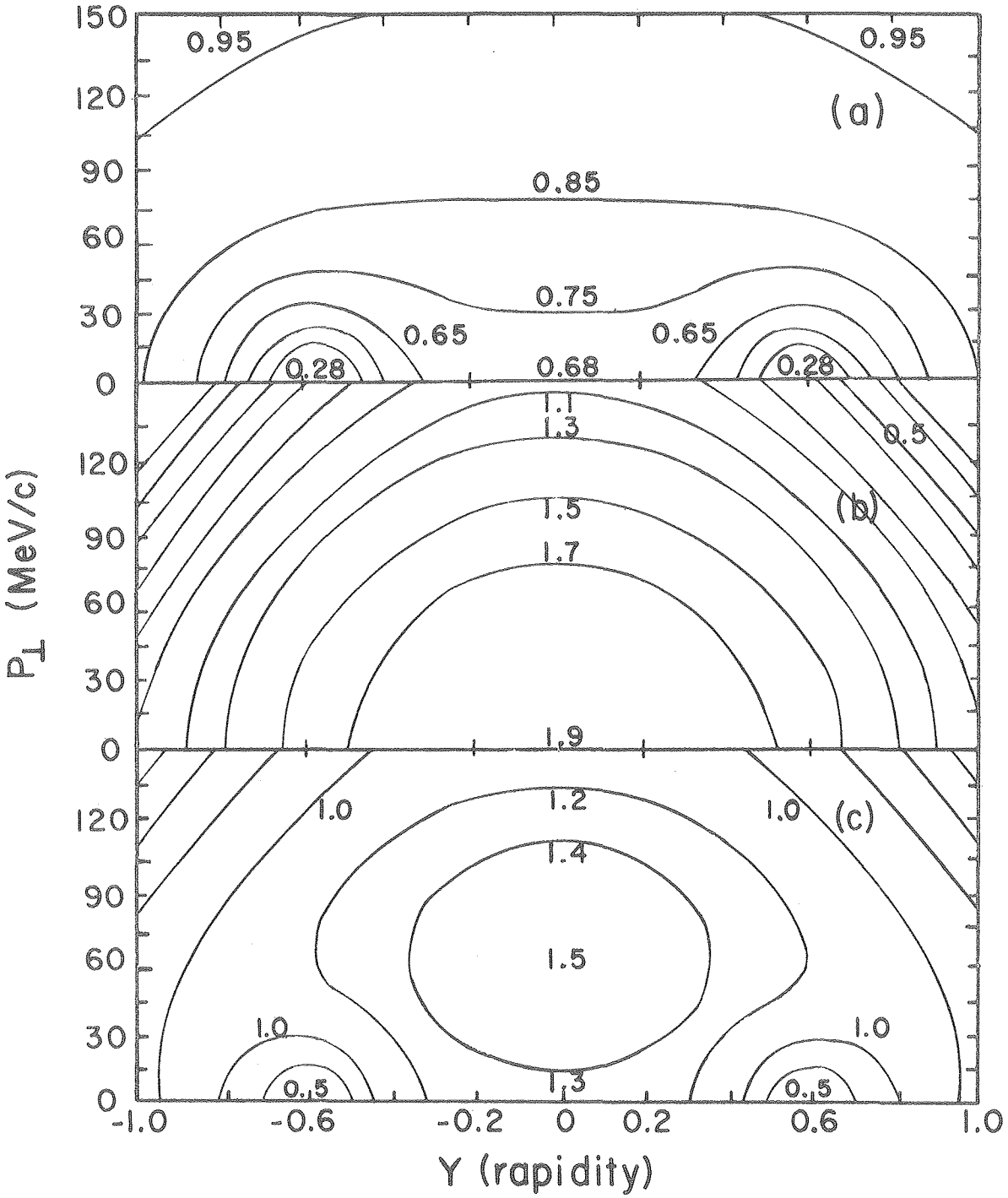

XBL 802-8092

Fig.III

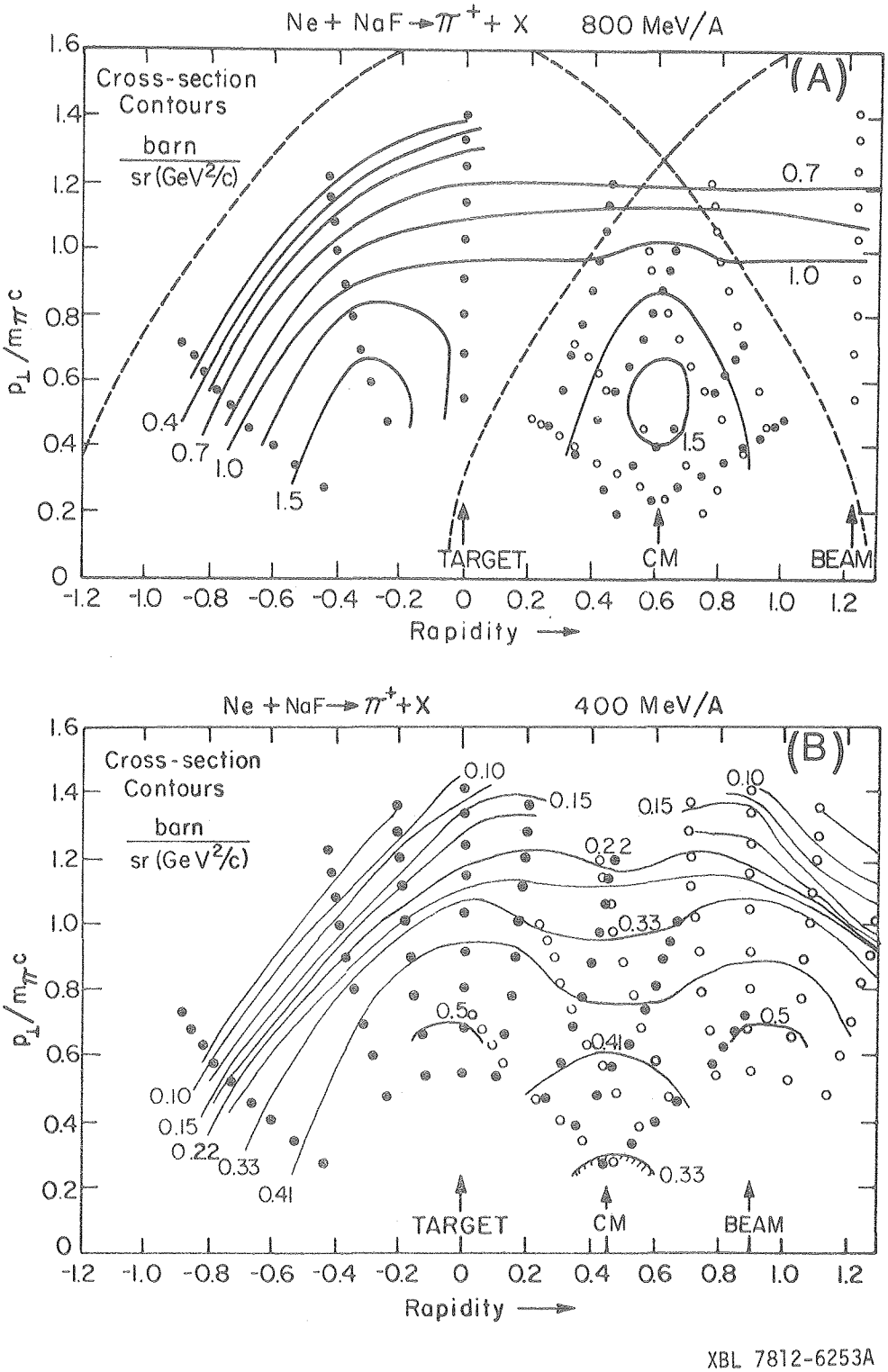
Ne + NaF → π⁺ + X 800 MeV/A
(A)
Cross-section Contours
barn / sr (GeV²/c)
0.4
0.7
1.0
1.5
0.7
1.0
1.5
TARGET
CM
BEAM
p⊥/mπc
Rapidity
Ne + NaF → π⁺ + X 400 MeV/A
(B)
Cross-section Contours
barn / sr (GeV²/c)
0.10
0.15
0.22
0.33
0.41
0.5
TARGET
CM
BEAM
p⊥/mπc
Rapidity
XBL 7812-6253A

Fig. IV

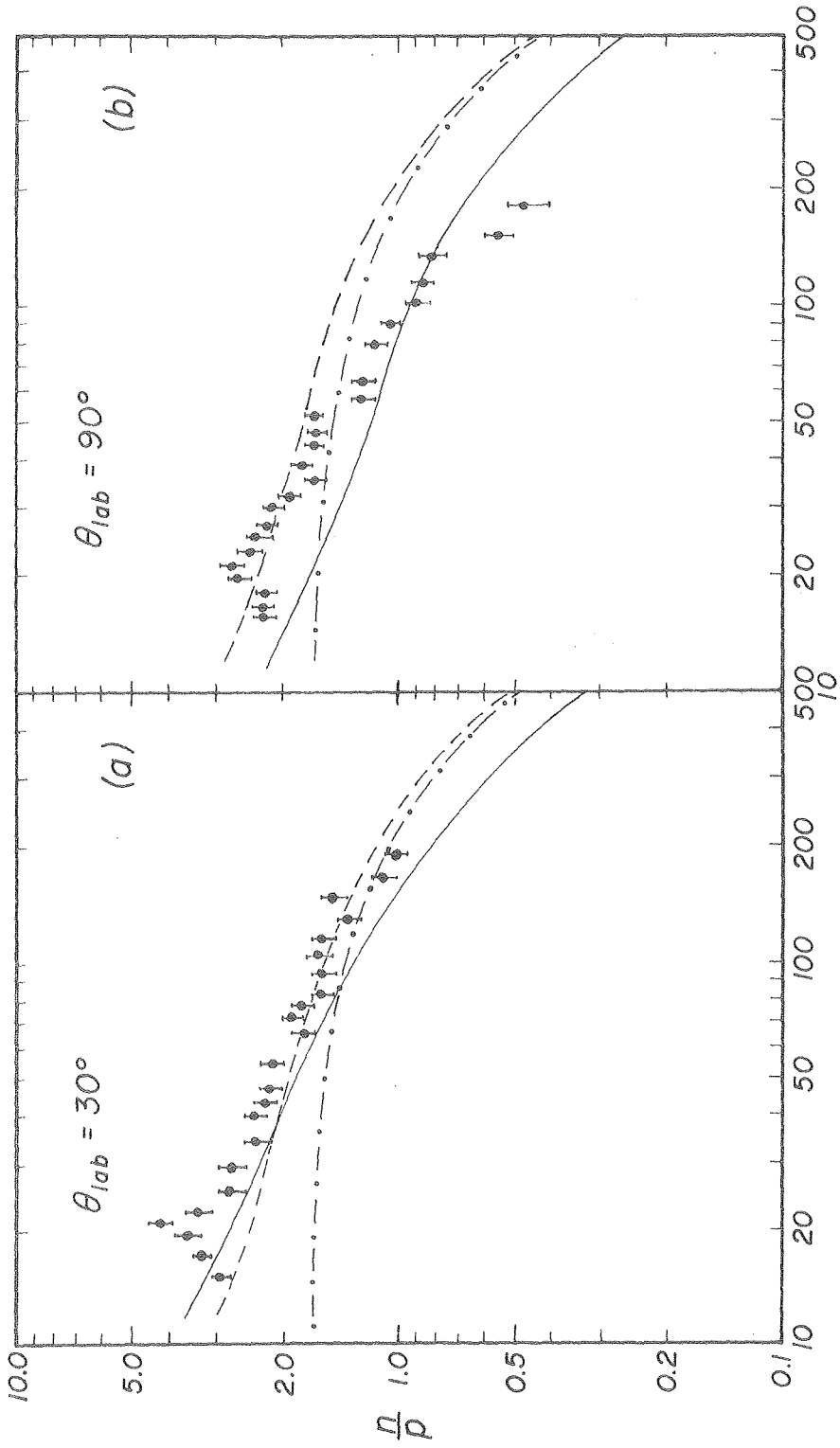

XBL 802-8095

Fig. V